International Journal of Scientific Research in Engineering and Management (IJSREM)
Volume: 10 Issue: 03 | March - 2026 SJIF Rating: 8.659 ISSN: 2582-3930

Green Synthesis of Manganese Dioxide Nanoparticles Using *Clitoria ternatea* Leaf Extract and Whey Milk

R. Antony Dyana Shiyanthini[1], Dr. J. Antony Rajam[2]

[1]*M.Sc Chemistry, Department of Chemistry, St. Mary's College (Autonomous) Affliated to Manonmaniam Sundaranar University, Thoothukudi-628001, Tamilnadu, India.*

[2]*Assistant Professor, Department of Chemistry, St. Mary's College (Autonomous) Affliated to Manonmaniam Sundaranar University, Thoothukudi-628001, Tamilnadu, India.*

Abstract

Green synthesis of manganese dioxide (MnO_2) nanoparticles was successfully carried out using *Clitoria ternatea* leaf extract (MnO_2–CT) and whey milk (MnO_2–W) as eco-friendly reducing and stabilizing agents. The synthesized nanoparticles were characterized using UV–Visible, FT-IR, XRD, FE-SEM, EDAX, and TGA analyses, confirming their nanoscale size, crystalline nature, surface functionalization, high purity, and good thermal stability. UV–Vis and FT-IR results verified nanoparticle formation and Mn–O bonding, while XRD indicated nanocrystalline structure with small crystallite size. Morphological studies revealed agglomerated, porous particles with high surface area. Thermal analysis showed that MnO_2–W exhibited higher stability, whereas MnO_2–CT displayed multistage decomposition due to phytochemical capping. Anticorrosion studies demonstrated enhanced protection, particularly in basic medium, with MnO_2–CT showing higher inhibition efficiency. Antibacterial evaluation against selected bacterial strains revealed moderate activity, with MnO_2–CT exhibiting slightly better performance due to synergistic effects of plant-derived compounds. Overall, the study highlights a sustainable and cost-effective approach for synthesizing multifunctional MnO_2 nanoparticles with promising applications in corrosion protection and antimicrobial activity.

Keywords: Green synthesis, Manganese dioxide nanoparticles, *Clitoria ternatea*, Anticorrosion, Antibacterial activity

1.INTRODUCTION

Manganese dioxide (MnO_2) is an important transition metal oxide widely used in catalysis, energy storage, and environmental applications. It occurs naturally as pyrolusite and can also be synthesized in different structural forms. Due to its low cost, abundance, and eco-friendly nature, it is highly valued in material science. MnO_2 shows polymorphism (α, β, γ, δ forms), which affects its properties like surface area and catalytic activity, and its strong redox nature makes it useful in batteries, supercapacitors, and wastewater treatment [1].

It is a black, odourless solid, insoluble in water and chemically reactive, forming compounds like potassium permanganate and manganese chloride. Structurally, it contains manganese in the +4 oxidation state arranged in different crystalline forms. MnO_2 is widely used in glass, ceramics, batteries, and as an oxidizing agent in organic reactions. It also plays a key role in modern applications such as supercapacitors, electrocatalysis, and sustainable energy storage, though challenges like low conductivity remain [2].

2.Materials and Methods

Biosynthesis Of Manganese Dioxide Nanoparticles Using *Clitoria Ternatea* Plant Extract

Clitoria ternatea was selected for the green synthesis of manganese dioxide (MnO_2) nanoparticles due to its rich phytochemical content, which acts as natural reducing and stabilizing agents. Fresh leaves were collected from a clean local area, washed, shade-dried and powdered. The leaf extract was prepared by boiling the powder in distilled water,

followed by filtration and storage. For nanoparticle synthesis, manganese acetate solution was mixed with the plant extract and heated, leading to a color change indicating nanoparticle formation. Sodium hydroxide was added to enhance precipitation and the mixture was further stirred, dried and calcined at high temperature to obtain MnO_2 nanoparticles, which were then stored for further use. The synthesized sample is named as MnO_2-CT.

Biosynthesis Of Whey Milk – Mediated Synthesis of Manganese Dioxide Nanoparticles

Whey milk was used as a natural reducing and stabilizing agent for the green synthesis of manganese dioxide (MnO_2) nanoparticles due to its content of proteins, lactose and other bioactive compounds. Fresh cow milk was collected and processed to obtain whey by heating and coagulating with lemon juice, followed by filtration. For nanoparticle synthesis, whey milk was diluted, heated and its pH was adjusted to neutral using sodium bicarbonate. Manganese acetate solution was then added and the mixture was heated further with pH adjustment using NaOH to promote nanoparticle formation. The resulting precipitate was filtered, dried and calcined at 500°C to obtain MnO_2 nanoparticles, which were then cooled and stored for further use. The synthesized sample is named as MnO_2-W.

Results and Discussion

UV-Visible Spectroscopy

UV-Visible analysis of MnO_2 – CT

The UV–Visible spectrum shows absorption bands at ~222 nm and ~248 nm, attributed to intrinsic O^{2-} → metal ion charge-transfer transitions, confirming the formation of the metal–oxygen lattice. A broad and intense absorption maximum at ~576 nm is associated with surface defect states and d–d electronic transitions of metal ions, indicating nanoscale crystallinity and possible mixed valence states. The broad visible-region absorption suggests particle size distribution and surface functionalization effects, enhancing optical activity. These features confirm the successful synthesis of nanostructured metal oxide with improved visible-light response, suitable for photocatalytic and optoelectronic applications [3].

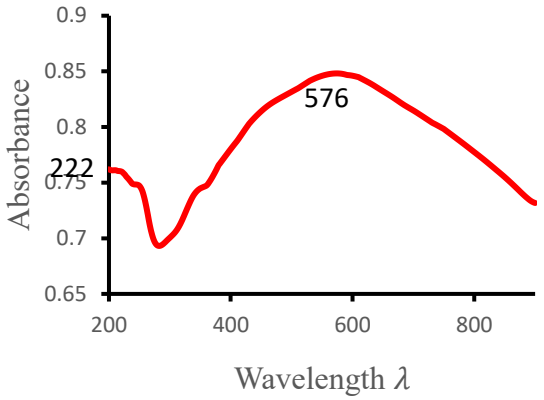

Figure -1: UV-Visible absorption spectrum of MnO_2 – CT Nanoparticles

UV-Visible analysis of MnO_2 – W

The UV–Visible absorption spectrum exhibits a prominent absorption peak at approximately 265 nm, which is attributed to intrinsic ligand-to-metal charge transfer (O^{2-} → metal ion) transitions, confirming the formation of the metal oxide framework. The broad absorption extending from the near-UV into the visible region indicates nanoscale particle formation, surface defect states and possible oxygen vacancies, which enhance light absorption over a wide wavelength range. The gradual decrease in absorbance toward higher wavelengths suggests particle size dispersion and surface-related electronic states rather than bulk behavior. Such optical characteristics are typical of metal oxide nanoparticles and are beneficial for applications in photocatalysis, sensing and optoelectronic devices due to improved visible-light harvesting [4].

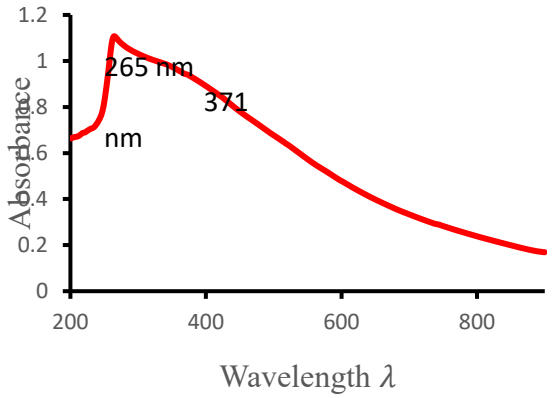

Figure -2: UV-Visible absorption spectrum of MnO_2 – W Nanoparticles

FT-IR analysis of MnO_2 - CT

The FT-IR spectrum of the MnO_2–CT sample confirms the presence of both surface functional groups and MnO_2 within the carbon matrix. A broad band around ~3400 cm^{-1} corresponds to O–H

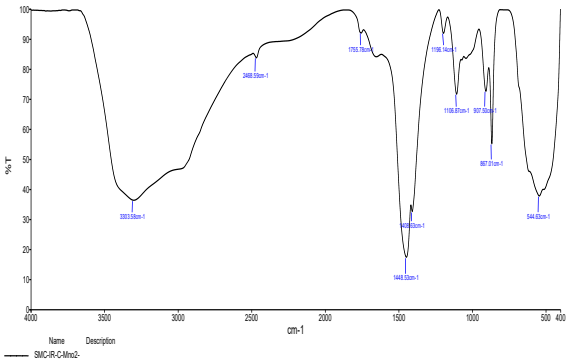

stretching vibrations from hydroxyl groups and adsorbed water, indicating hydrophilic surface characteristics due to bio-capping agents. Weak peaks in the ~1600–1800 cm^{-1} range are attributed to C=O and C=C stretching of oxygen-containing carbon groups or residual phytochemicals, which enhance interaction between MnO_2 and the carbon support. Strong absorption bands in the ~500–600 cm^{-1} region are assigned to Mn–O and O–Mn–O lattice vibrations, confirming the formation of MnO_2. Overall, the observed FT-IR bands are consistent with reported studies on green-synthesized MnO_2 nanoparticles [5].

Figure -3: FT-IR Spectrum of MnO_2 -CT Nanoparticles

FT-IR analysis of MnO_2 – W

The FT-IR spectrum of the MnO_2–W sample confirms the successful green synthesis of MnO_2 nanoparticles along with the presence of phytochemical surface groups. A broad band at ~3377 cm^{-1} is attributed to O–H stretching from hydroxyl groups and adsorbed water, indicating bio-capping effects. Peaks at ~2920 cm^{-1} and ~2853 cm^{-1} correspond to C–H stretching of aliphatic compounds from plant-derived biomolecules. The band near ~2330 cm^{-1} is linked to absorbed CO_2 or related overtones. The peak at ~1489 cm^{-1} represents C=C vibrations of aromatic or conjugated compounds, showing interaction with the MnO_2 surface, while the

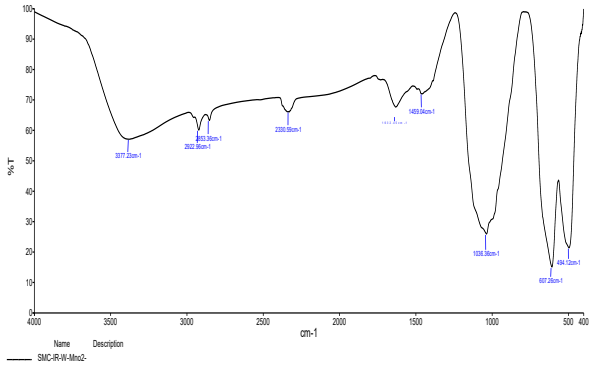

~1023 cm^{-1} band is due to C–O stretching of alcohols or phenolics, confirming surface functionalization. Strong bands at ~607 cm^{-1} and ~484 cm^{-1} are assigned to Mn–O and O–Mn–O vibrations, providing clear evidence of MnO_2 formation. Overall, these results agree with reported FT-IR studies of green-synthesized manganese oxide nanoparticles [6].

Figure -4: FT-IR Spectrum of MnO_2 – W Nanoparticles

XRD analysis of MnO_2 – CT

The XRD pattern of the synthesized MnO_2 sample, recorded using Cu Kα radiation over a 2θ range of 10–80°, confirms its crystalline structure. Distinct diffraction peaks at ~13°, 25°, 32°, 37°, 42°, 50°, 57°, 60°, 65°, and 69° match standard MnO_2 data, indicating the formation of a pure phase without impurities. The broadened peaks suggest a nanocrystalline nature due to small crystallite size and

possible lattice strain. The average crystallite size, calculated using the Scherrer equation, falls within the nanometer range, confirming nanoparticle formation. The absence of peak shifts suggests minimal lattice distortion, indicating good crystallinity of the MnO_2 nanoparticles. The good agreement of peak positions with standard data also indicates a well-ordered crystal structure, which contributes to the stability and reliability of MnO_2 nanoparticles in practical applications. Overall, these nanostructured MnO_2 materials exhibit properties suitable for applications in catalysis, energy storage and environmental remediation [7].

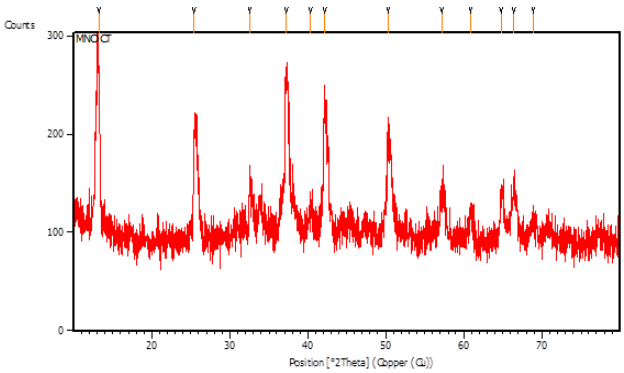

Figure -5: XRD Spectrum of MnO_2 – CT Nanoparticles

XRD analysis of MnO_2 – W

The XRD pattern of the MnO_2–W sample, recorded using Cu Kα radiation over a 2θ range of 10–80°, confirms its crystalline nature. The diffraction peaks observed around 30–40° and near 60° match standard MnO_2 data, verifying the formation of the MnO_2 phase. The absence of extra peaks indicates good phase purity without impurities. Broad diffraction peaks suggest a nanocrystalline structure, likely due to small crystallite size and structural disorder from the synthesis process. The average crystallite size, calculated using the Scherrer equation, is about 2.23 nm. The very small crystallite size (~2.23 nm) suggests a high surface-to-volume ratio, enhancing reactivity and performance in applications. The consistent peak positions indicate good crystallographic stability of the MnO_2 phase. This nanostructured MnO_2 is expected to exhibit enhanced surface properties, making it suitable for applications in catalysis, energy storage and environmental remediation [7].

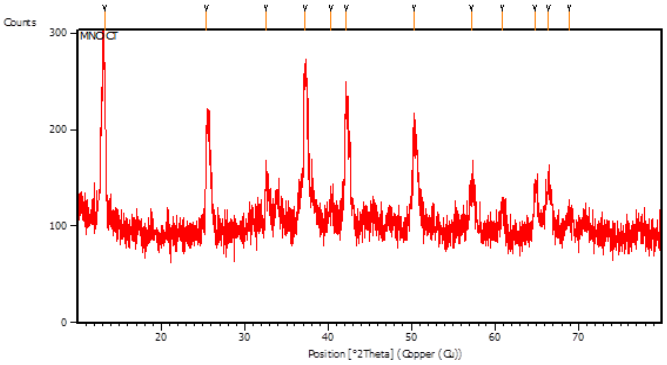

Figure -6: XRD Spectrum of MnO_2 -W Nanoparticles

FE-SEM analysis of MnO_2 – CT

FE-SEM images show MnO_2 nanoparticles with nearly spherical to irregular shapes and some agglomeration due to high surface energy. The particles are uniformly distributed with a rough, porous surface, indicating high surface area. A distinct flower-like morphology with radially arranged needle-shaped structures forming ~5 μm clusters is observed, suggesting hierarchical structures beneficial for catalytic and surface-related applications [8].

Figure -7: FE-SEM images of MnO_2 – CT Nanoparticles in different magnification a) 5 μm b) 2 μm c) 5 μm d) 10 μm e) 20 μm f) 50 μm

FE-SEM analysis of MnO_2 – W

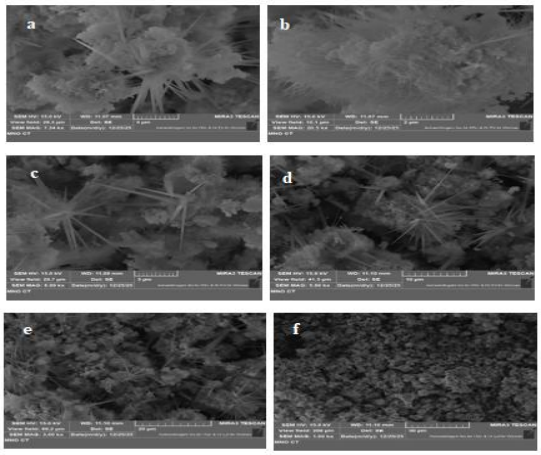

The FE-SEM micrograph shows nanostructured particles with irregular to quasi-spherical shapes and noticeable agglomeration due to strong interparticle interactions. The particles are uniformly distributed, indicating consistent nucleation and growth. The rough, porous surface suggests high surface area, making the material suitable for catalysis, sensing and energy storage. The absence of large crystals or secondary phases confirms controlled particle formation, consistent with reported metal oxide nanomaterials [9].

Fig -8: FE-SEM images of MnO_2-W Nanoparticles in different magnification a) 5 μm b) 2 μm c) 5 μm d) 10 μm e) 20 μm f) 50 μm

EDAX analysis of MnO_2 – CT

The EDAX spectrum confirms that the

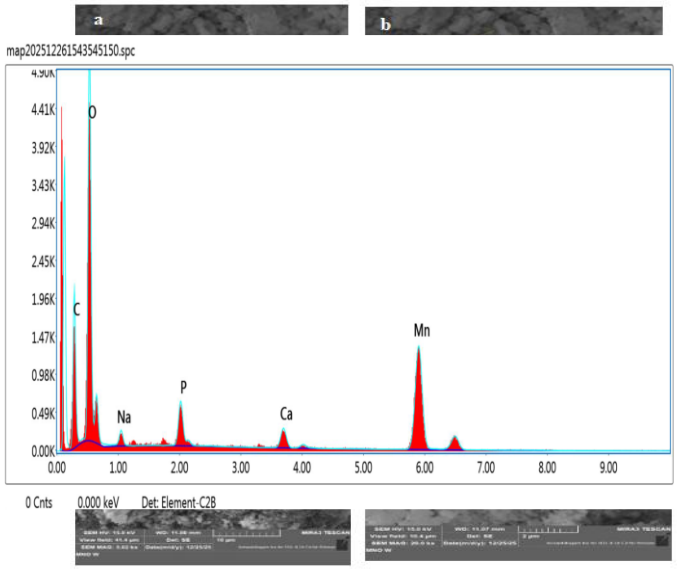

synthesized material mainly consists of manganese (Mn) and oxygen (O), indicating successful formation of manganese oxide as the primary phase. The strong oxygen peak reflects effective metal–oxygen bonding within the structure. Minor signals of sodium (Na) and potassium (K) are present, likely due to residual precursor salts or plant-based compounds from the synthesis process. A weak carbon peak is also observed, which can be attributed to surface-bound organic matter or the carbon tape used during analysis. The absence of other impurity peaks suggests high purity of the material. Overall, the EDAX results, along with quantitative data, validate the successful synthesis and are consistent with previously reported studies on manganese oxide nanomaterials [10].

Figure -9: EDAX Spectrum of MnO_2 – CT Nanoparticles

EDAX analysis of MnO_2 – W

The EDAX analysis confirms that the synthesized sample is primarily composed of manganese (Mn) and oxygen (O), verifying the successful formation of manganese oxide with strong metal–oxygen bonding. Minor peaks of sodium (Na), calcium (Ca), and phosphorus (P) are also observed, likely originating from residual precursors, mineral content, or plant-based compounds used in the synthesis process. A weak carbon signal is attributed to surface-adsorbed organic matter or the carbon tape used during analysis. The absence of significant impurity peaks

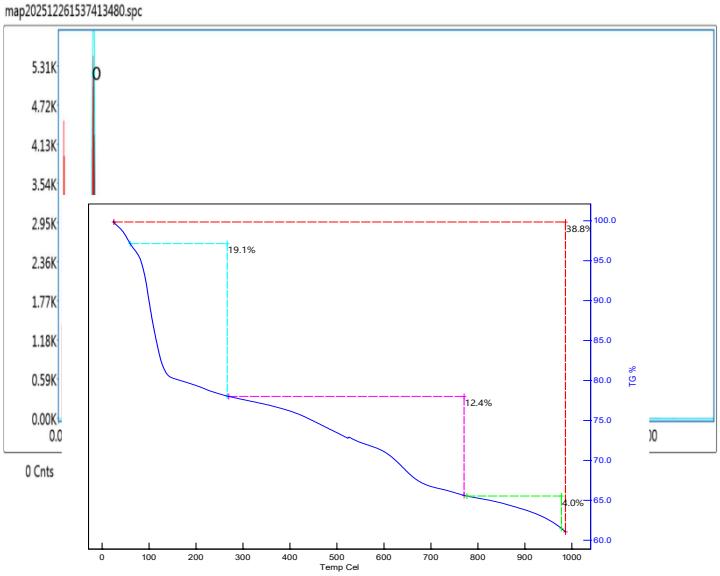

indicates good purity and controlled synthesis. Overall, the elemental composition data supports successful material formation and is consistent with previously reported manganese oxide nanomaterials [10].

Figure -10: EDAX Spectrum of MnO_2 – W Nanoparticles

TGA analysis of MnO_2 – CT

The TGA analysis of green-synthesized MnO_2 nanoparticles shows a clear three-stage weight loss pattern, indicating gradual thermal decomposition

along with good thermal stability. The first weight loss (~19.1%) up to 300 °C is due to the removal of adsorbed water and decomposition of plant-derived organic compounds from *Clitoria ternatea*. A second weight reduction (~12.4%) between about 300 °C and 800 °C is attributed to the breakdown of remaining organic residues and partial structural changes in the MnO_2 lattice. At higher temperatures (800–1000 °C), a small weight loss (~4.0%) occurs, likely due to phase transformations of MnO_2 into lower oxides and the release of lattice oxygen. Overall, the nanoparticles retain around 61.2% of their mass up to 1000 °C, confirming good thermal stability. The total weight loss (~38.8%) results from moisture removal, organic decomposition, and structural changes, while the multi-step degradation behavior reflects the presence of phytochemical capping that enhances stability but decomposes gradually with temperature [11].

Figure -11: TGA curve of MnO_2 – CT Nanoparticles

Combined TG-DTA-DTG

The TG–DTA–DTG analysis shows a multi-step thermal decomposition from room temperature to ~900 °C. An initial weight loss below 150 °C is due to moisture removal. Between 150–400 °C, gradual mass loss occurs from decomposition of organic capping agents. A smaller peak around 550–650 °C indicates removal of residual carbon and structural rearrangement of the oxide. Above 650 °C, minimal weight change confirms the formation of a stable inorganic oxide, demonstrating good thermal stability [12].

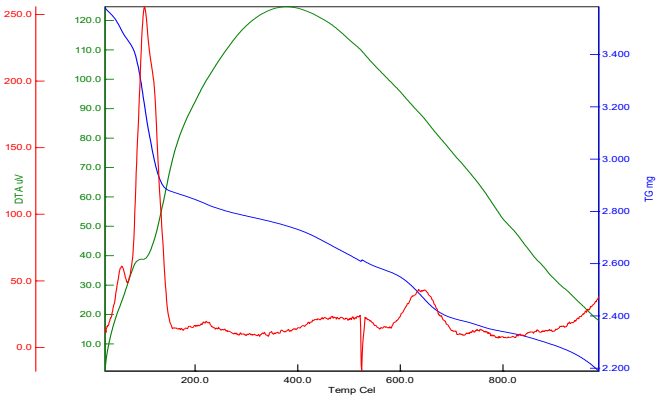

Figure -12: TG-DTA-DTG curve of MnO_2 – CT Nanoparticles

TGA analysis of MnO_2 – W

The TGA curve of MnO_2 nanoparticles shows very low overall weight loss (~5%), indicating excellent thermal stability and high purity. An initial loss (~1.6%) below 120 °C is due to moisture removal. From 120–900 °C, only minimal weight change occurs, reflecting strong structural stability and low organic residue content. A small additional loss (~2.4%) above 900 °C is attributed to phase changes or oxygen loss, possibly forming lower manganese oxides. The minimal weight loss over a wide temperature range indicates strong Mn–O

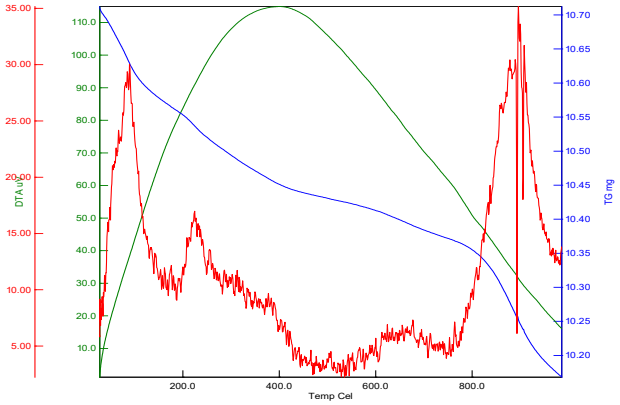

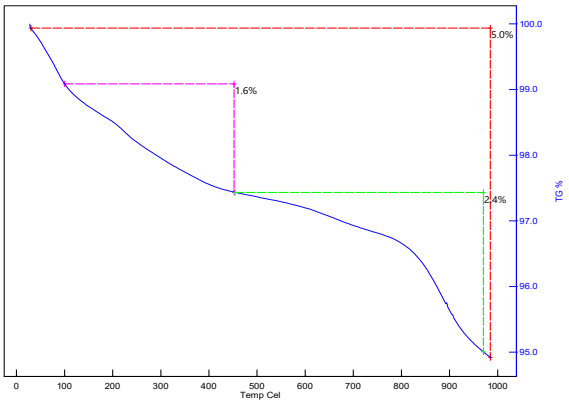

bonding within the lattice, contributing to the material's high thermal robustness and structural integrity. The observed thermal behavior suggests that the nanoparticles are suitable for high-temperature applications such as catalysis, energy storage and electrochemical devices due to their stability and low decomposition rate [1].

Figure -13: TGA curve of MnO_2 -W Nanoparticles

Combined TG-DTA-DTG

The TG–DTA–DTG thermogram shows

multi-step thermal decomposition from room temperature to ~900 °C, with gradual mass loss from ~10.70 mg to ~10.18 mg. An initial loss below 150 °C is due to removal of adsorbed water and surface hydroxyl groups. Between 150–400 °C, weight loss occurs from decomposition of organic capping agents. From 400–650 °C, slower mass reduction indicates removal of residual carbon and structural rearrangement of the oxide. A final peak around 850–880 °C suggests phase transformation, after which the material remains thermally stable [12].

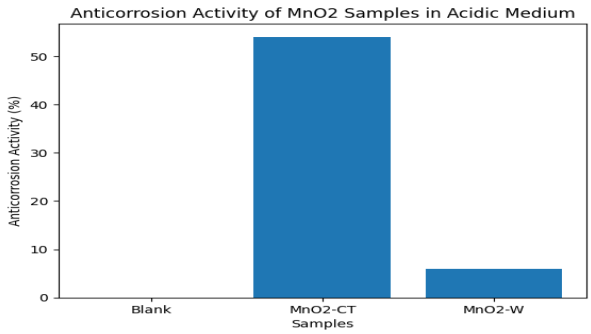

Figure -14: TG-DTA-DTG curve of MnO_2 – W Nanoparticles

Applications

Anticorrosion activity

The anticorrosion behavior of the synthesized samples was studied in acidic, basic, and neutral media using the weight loss method. Results show that in acidic medium, MnO_2-CT provides higher inhibition efficiency (up to 54%), while MnO_2-W exhibits a lower corrosion rate. In basic medium, the anticorrosion performance is highest, with MnO_2-CT achieving up to 80% efficiency, indicating strong protection. In neutral medium, the performance is comparatively lower, though MnO_2-W shows better stability with the lowest corrosion rate (0.52). Overall, the materials perform best in basic medium, followed by acidic, and least in neutral conditions.

Anticorrosion activity in acidic medium

Medium	W_1	W_2	ΔW (g)	Corrosion % rate $\left[\frac{W_1-W_2}{W_1}\right] \times 100$	Anticorrosion activity in percentage (%) $\left[\frac{CR_b-CR_n}{CR_b}\right] \times 100$
Blank	7.7387	7.6433	0.0954	1.23	-
MnO_2-CT	7.6770	7.6255	0.0895	1.17	54
MnO_2-W	7.6940	7.5875	0.0685	0.89	6

Figure -15: Anticorrosion activity of MnO_2 samples in acidic medium

Anticorrosion activity in basic medium

Medium	W_1	W_2	ΔW (g)	Corrosion % rate $\left[\frac{W_1-W_2}{W_1}\right] \times 100$	Anticorrosion activity in percentage (%) $\left[\frac{CR_b-CR_n}{CR_b}\right] \times 100$
Blank	7.5986	7.4013	0.1973	2.60	-
MnO_2-CT	7.6903	7.5981	0.0922	1.20	80
MnO_2-W	7.6947	7.5601	0.1346	1.75	47

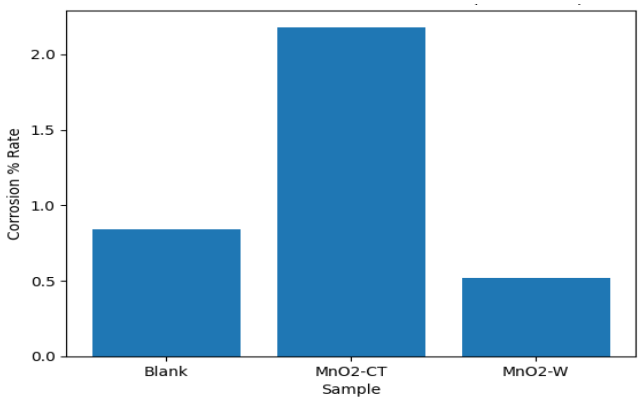

Figure -16: Anticorrosion activity of MnO_2 samples in basic medium

Corrosion rate of MnO_2 samples

Medium	W_1	W_2	$\Delta W\ (g)$	Corrosion % rate $\left[\frac{W_1 - W_2}{W_1}\right] \times 100$
Blank	7.6003	7.6638	0.0635	0.84
MnO_2-CT	7.7114	7.5436	0.1678	2.18
MnO_2-W	7.6653	7.6253	0.0400	0.52

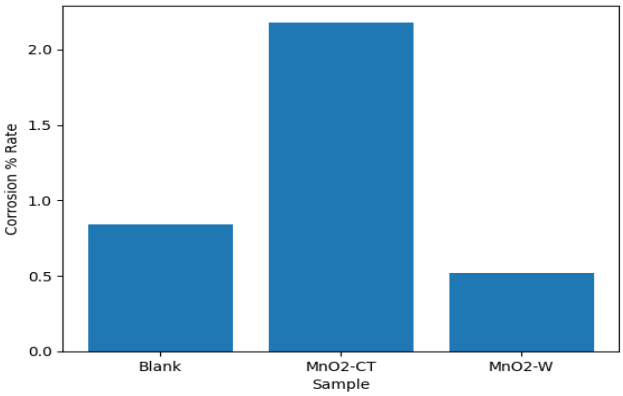

Figure -17: Corrosion rate of MnO_2 samples

Antibacterial activity

The antibacterial activity of MnO_2-W and MnO_2-CT was evaluated against selected bacteria and compared with ciprofloxacin. The standard antibiotic showed the highest inhibition zones (21–27 mm), while both MnO_2 samples exhibited moderate activity (6–12 mm). Among them, MnO_2-CT demonstrated slightly better antibacterial effects than MnO_2-W, especially against *Klebsiella pneumoniae*. This enhanced activity is likely due to phytochemicals from *Clitoria ternatea* providing a synergistic effect with MnO_2 nanoparticles. Overall, MnO_2-CT shows better antibacterial potential than MnO_2-W.

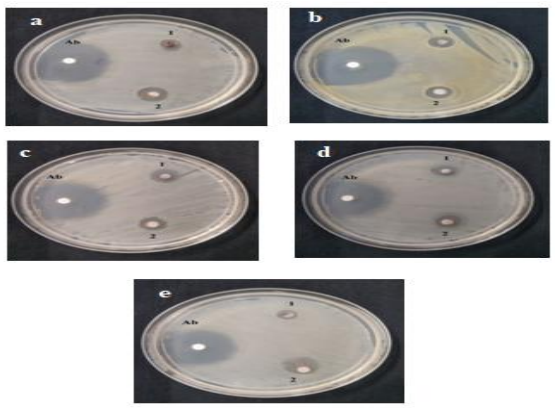

Figure -18: Antibacterial activity of MnO_2-CT, MnO_2-W Nanoparticles

Bacteria	Inhibition zone in mm		
	Ab ciprofloxacin	MnO_2-W	MnO_2-CT
a) *E.coli*	27	8	10
b) *Staphylococcus aureus*	21	8	9
c) *Bacillus subtilis*	25	9	9
d) *Bacillus cereus*	22	8	9
e) *Kleibsiella pneumonia*	23	6	12

3.CONCLUSION

This study demonstrates the eco-friendly synthesis of MnO_2 nanoparticles using *Clitoria ternatea* leaf extract (MnO_2–CT) and honey (MnO_2–W) as natural reducing and stabilizing agents. The synthesized nanoparticles were characterized using various techniques and evaluated for antibacterial, anticorrosion, and food preservation applications. UV–Vis analysis confirmed nanoparticle formation, while FT-IR indicated Mn–O vibrations along with phytochemical capping. XRD revealed crystalline structures with very small crystallite sizes, and FE-SEM showed agglomerated, nanosized particles with rough morphology. EDX confirmed the presence of

Mn and O with high purity. TGA results indicated good thermal stability, with MnO_2–W being more stable and MnO_2–CT showing multi-stage weight loss due to phytochemicals. Anticorrosion studies showed improved protection, especially in basic medium. Antibacterial tests against multiple strains demonstrated moderate activity, with MnO_2–CT performing slightly better due to synergistic effects of plant compounds. Overall, the results confirm that green synthesis using plant and natural products is a sustainable and effective method for producing multifunctional MnO_2 nanoparticles with promising practical applications.

ACKNOWLEDGEMENT

I would like to express my gratitude to my primary supervisor, Dr. J. Antony Rajam, who guided me throughout this research article. I would also like to thank my friends and family who supported me and offered deep insight into the study.

REFERENCES

1. Wei, W., Cui, X., Chen, W., & Ivey, D. G., Manganese oxide-based materials as electrochemical supercapacitor electrodes, Vol. 40, UK, 2011, 1697–1721.
2. Greenwood, N. N., & Earnshaw, A., Chemistry of the Elements, 2nd ed., UK, 1997.
3. Xu, C., Li, B., & Du, H., Nanostructured manganese oxide for electrochemical energy storage and optical applications, Vol. 8, USA, 2012, 104–112.
4. Zhang, L., & Xia, Y., Metal oxide nanoparticles: optical properties and applications, Vol. 6, USA, 2013, 221–230.
5. Wang, Y., Zhang, X., & Li, H., Green synthesis and characterization of manganese oxide nanoparticles using plant extracts, Vol. 10, USA, 2015, 45–52.
6. Ahmed, S., Ahmad, M., Swami, B. L., & Ikram, S., A review on plants extract mediated synthesis of silver nanoparticles for antimicrobial applications, Vol. 7, India, 2016, 17–28.
7. Post, J. E., Manganese oxide minerals: Crystal structures and economic and environmental significance, Vol. 96, USA, 1999, 3447–3454.
8. Zhang, X., Chen, Y., & Liu, H., Flower-like MnO_2 nanostructures: synthesis and catalytic applications, Vol. 8, USA, 2015, 210–218.
9. Xia, H., Wang, Y., & Lin, J., Nanostructured metal oxides for advanced functional applications, Vol. 6, USA, 2012, 120–128.
10. Goldstein, J., Newbury, D., Joy, D., Lyman, C., Echlin, P., Lifshin, E., Sawyer, L., & Michael, J., Scanning Electron Microscopy and X-ray Microanalysis, 3rd ed., USA, 2003.
11. Singh, J., Dutta, T., Kim, K. H., Rawat, M., Samddar, P., & Kumar, P., Green synthesis of metals and their oxide nanoparticles: Applications for environmental remediation, Vol. 36, USA, 2018, 1–15.
12. Vyazovkin, S., Burnham, A. K., Criado, J. M., Pérez-Maqueda, L. A., Popescu, C., & Sbirrazzuoli, N., ICTAC kinetics committee recommendations for performing kinetic computations on thermal analysis data, Vol. 520, Netherlands, 2011, 1–19.